Then, H. L. (2006). Foreground contamination of the WMAP CMB maps from the perspective of the matched circle test. Monthly Notices of the Royal Astronomical Society, 373(1), 139-145. DOI: 10.1111/j.1365-2966.2006.11035.x

Mon. Not. R. Astron. Soc. **373,** 139–145 (2006) doi:10.1111/j.1365-2966.2006.11035.x

Foreground contamination of the *WMAP* CMB maps from the perspective of the matched circle test

H. Then★

Abteilung Theoretische Physik, Universität Ulm, Albert-Einstein-Allee 11, 89069 Ulm, Germany

Accepted 2006 August 25. Received 2006 July 12; in original form 2005 November 25

ABSTRACT

Wilkinson Microwave Anisotropy Probe has provided cosmic microwave background (CMB) maps of the full sky. The raw data are subject to foreground contamination, in particular near to the Galactic plane. Foreground-cleaned maps have been derived, e.g. the internal linear combination map of Bennett et al., and the reduced foreground TOH map of Tegmark et al. Using *S* statistics, we examine whether residual foreground contamination is left over in the foreground-cleaned maps. In particular, we specify which parts of the foreground-cleaned maps are sufficiently accurate for the circle-in-the-sky signature. We generalize the *S* statistic, called *D* statistic, such that the circle test can deal with CMB maps in which the contaminated regions of the sky are excluded with masks.

Key words: methods: data analysis – methods: statistical – cosmic microwave background – cosmology: miscellaneous – large-scale structure of Universe.

1 INTRODUCTION

Astronomical observations of recent years have answered a number of fundamental questions. A cornerstone in revealing the state of the Universe was the combination of observations at low redshift (clusters, including the mass-to-light method, baryon fraction and cluster abundance evolution), intermediate redshift (SNe), and high redshift [cosmic microwave background (CMB)] (Bahcall et al. 1999). On the other hand, many new fundamental questions were raised, e.g. questions concerning dark matter and dark energy. Moreover, many answers depend sensitively on the accuracy of the observations, e.g. on the accuracy of the curvature which determines whether we live in an *exactly* flat universe or a slightly curved one.

Concerning the high-redshift observations, the temperature fluctuations in the CMB are subject to systematic errors resulting from foreground contamination. In particular, near to the Galactic plane, the CMB maps are highly contaminated by radiation from the Milky Way. Fortunately, there exist methods to reduce the foreground contamination in the maps (Tegmark & Efstathiou 1996; Bennett et al. 2003). A growing number of foreground-cleaned maps are available (Bennett et al. 2003; Tegmark, de Oliveira-Costa & Hamilton 2003; Eriksen et al. 2004; Hinshaw et al. 2006) and the reader may ask which of them comes closest to the genuine temperature fluctuations of the CMB. This question is related to the question how reliable the maps are, especially near to the Galactic plane. There is no way to decide whether a given pixel of a map displays the correct temperature (apart from pixels that are really very off in their values), because the genuine temperature fluctuations of the CMB are unknown. However, taking ensembles of pixels, it is possible to check statistically whether the spatial temperature distribution agrees with statistical isotropy. In this paper, we perform such checks using *S* statistic and a generalization of it. The result is that even for the best available CMB map either there is left residual foreground contamination or the angular resolution is significantly reduced. Because of this residual foreground contamination, we extend the definition of the *S* statistic such that the foreground-contaminated regions of the sky can be excluded. For further studies, this might open a new chance for the detection of matched circles as a result of the non-trivial topology of the Universe.

★E-mail: holger.then@uni-ulm.de

2 *D* STATISTIC

S statistic was initially introduced by Cornish, Spergel & Starkman (1998) for the search of correlated pairs of circles in the CMB sky,

$$S = \frac{\langle 2\delta T_1(\pm\phi)\delta T_2(\phi+\phi_*)\rangle}{\langle \delta T_1(\phi)^2 + \delta T_2(\phi)^2\rangle}, \quad (1)$$

where $\delta T_i(\phi)$ $(i = 1, 2)$ denotes the CMB temperature fluctuations on two circles 1 and 2, and $\langle\cdot\rangle = \int_0^{2\pi} \mathrm{d}\phi$ is the integration along the two circles of equal radius with relative phase ϕ_*.

We generalize the definition of the *S* statistic to include pixel weights that specify the certainty, respectively, uncertainty of the temperature fluctuations. The new statistic is called *D* statistic. In addition, we note that the *D* statistic is not restricted to correlations along circles, but can be used along arbitrary curves γ.

Definition 1. Let γ_1 and γ_2 be curves parametrized by ϕ, $\phi \in [0, 2\pi]$, and $w(\gamma_i)$ be positive pixel weights that specify how accurate the CMB temperature fluctuations $\delta T(\gamma_i)$ are known at $\gamma_i = \gamma_i(\phi)$.

Using the notation

$$\langle\langle f(\gamma_1,\gamma_2)\rangle\rangle := \int_0^{2\pi} \mathrm{d}\phi\, f(\gamma_1(\phi),\gamma_2(\phi)) \times \sqrt{w(\gamma_1(\phi))w(\gamma_2(\phi))\left|\tfrac{\mathrm{d}}{\mathrm{d}\phi}\gamma_1(\phi)\right|\left|\tfrac{\mathrm{d}}{\mathrm{d}\phi}\gamma_2(\phi)\right|},$$

we call

$$D := \frac{\langle\langle 2\delta T(\gamma_1)\delta T(\gamma_2)\rangle\rangle}{\langle\langle \delta T(\gamma_1)^2+\delta T(\gamma_2)^2\rangle\rangle} \tag{2}$$

D statistic.

We remark that the D statistic is invariant if the weights are rescaled, i.e. $w(\gamma_i(\phi)) \mapsto cw(\gamma_i(\phi))$, where c is a positive constant. The same is also true if the temperatures are rescaled.

The pixel weights may be expressed by $w = (1+1/\xi)^{-1}$, where ξ is the signal-to-noise ratio. If a temperature fluctuation is known exactly, the corresponding weight equals to 1. In the other extreme, i.e. when δT is not known at all, its weight vanishes.

It is allowed to parametrize the curves γ_i arbitrarily, but care has to be taken if the ratio between $|\frac{\mathrm{d}}{\mathrm{d}\phi}\gamma_1(\phi)|$ and $|\frac{\mathrm{d}}{\mathrm{d}\phi}\gamma_2(\phi)|$ varies with ϕ, because the D statistic depends on the parametrization. We will always choose the parametrization such that $|\frac{\mathrm{d}}{\mathrm{d}\phi}\gamma_i(\phi)| =$ constant allowing us to drop the factors $|\frac{\mathrm{d}}{\mathrm{d}\phi}\gamma_i(\phi)|$ in the definition of the D statistic.

If one chooses the curves γ_1 and γ_2 to be circles of the same radius and sets all pixel weights equal to 1, one recovers equation (1) as a special case of equation (2).

The D statistic always takes values between $D=-1$, maximal *anticorrelation*, and $D=1$, maximal *correlation*. In a typical resolution-limited application, the D statistic has a value distribution that is centred near

$$D_{\mathrm{peak}} = \frac{\chi^2}{1+\chi^2} \tag{3}$$

and has

$$\mathrm{FWHM} \simeq \sqrt{\frac{8\ln 2}{N_0}} \tag{4}$$

for N_0 large, where N_0 is the number of *independent* pixels (Cornish et al. 1998). χ is the correlation ratio,

$$\chi^2 = \frac{A_{\mathrm{corr}}^2}{A^2 - A_{\mathrm{corr}}^2}, \tag{5}$$

where A_{corr} stands for the mean amplitude of the correlated part of the signal, and A for the mean amplitude of the total signal including the detector noise, i.e. $A^2 = A_{\mathrm{corr}}^2 + A_{\mathrm{uncorr}}^2 + A_{\mathrm{noise}}^2$.

Moreover, we also take angular weights into consideration. In particular, we emphasize that we always remove the DC and the lowest frequency AC components along each curve γ_i, cf. Appendix A. Especially in Section 5, we use the angular weights of Cornish et al. (2004).

3 THE METHOD

Observing the CMB over the full sky, one is confronted with foreground emission of our own galaxy that strongly contaminates the temperature fluctuations near to the Galactic plane. A quantitative measure of this foreground contamination can be obtained from the D statistic by choosing γ_1 to be a closed path and setting $\gamma_2(\phi) = \gamma_1(\phi_* - \phi)$. In the subcase of circles, we call this set up *front-to-front* circles, because γ_2 traverses the same circle as γ_1, but in the opposite direction.

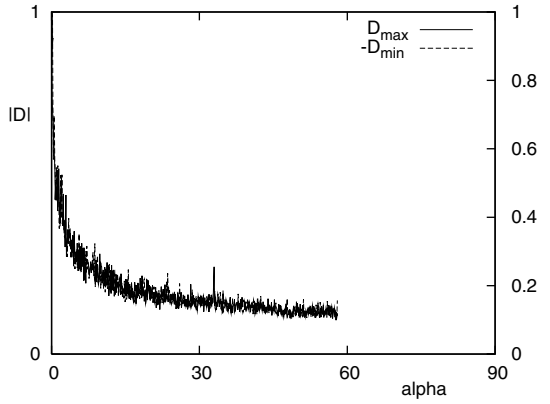

Figure 1. D statistic of the foreground-cleaned W-band map where the extremal D-values, i.e. D_{max} and $-D_{\mathrm{min}}$, are plotted for front-to-front circles that are parallel to the Galactic plane. α is the circle radius. Restricting to $\alpha < 58^\circ$, the Galactic foreground contamination is not displayed. The extragalactic contamination is quite negligible, since it does not destroy the symmetry between D_{max} and D_{min}.

Our working hypothesis is that for almost all points on the sky there are temperature fluctuations in the CMB on all scales and that the cosmological principle holds. Consequently, we do not expect any correlations in the genuine temperature fluctuations, i.e. $A_{\mathrm{corr}} = 0$, apart from the circle-in-the-sky signature in case of a non-trivial topology of the Universe. In other words, the typical temperature fluctuations of the CMB should result in a D statistic that is symmetric around $D_{\mathrm{peak}} = 0$. That this expectation indeed holds is shown with front-to-front circles that are far away from the Galactic plane, see Fig. 1. [All figures in this section, namely Figs 1–3, were made with the foreground-cleaned W-band map of the first year *Wilkinson Microwave Anisotropy Probe* (*WMAP*) data (Bennett et al. 2003). More details about the CMB maps can be found in Section 4.] What we actually plot in Fig. 1 is not a histogram of the D-values, but $-D_{\mathrm{min}} := -\min_{\phi_*} D$ and $D_{\mathrm{max}} := \max_{\phi_*} D$ in dependence of the circle radius α. Being symmetric around $D_{\mathrm{peak}} = 0$, the smallest and largest quantities of a finite set of D-values have similar size, except of their opposite signs, i.e. $-D_{\mathrm{min}} \approx D_{\mathrm{max}}$. In short, we call this to be a *symmetry* between D_{min} and D_{max}. In Fig. 1, we see also that the width of the distribution which is related to the sum of $-D_{\mathrm{min}} + D_{\mathrm{max}}$ decreases monotonically with increasing radius α of

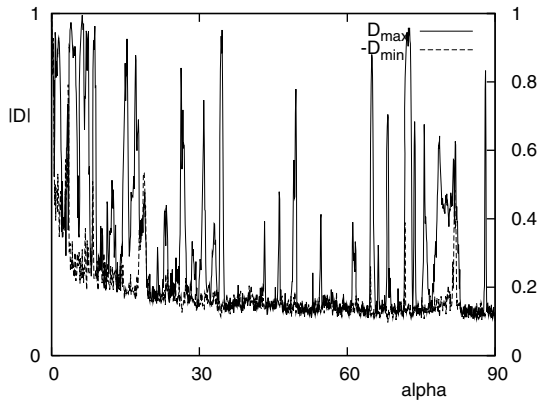

Figure 2. D statistic of the foreground-cleaned W-band map where the front-to-front circles cross the Galactic plane perpendicular. The peaks in D_{max} and the asymmetry between D_{max} and D_{min} result from Galactic foreground contamination.

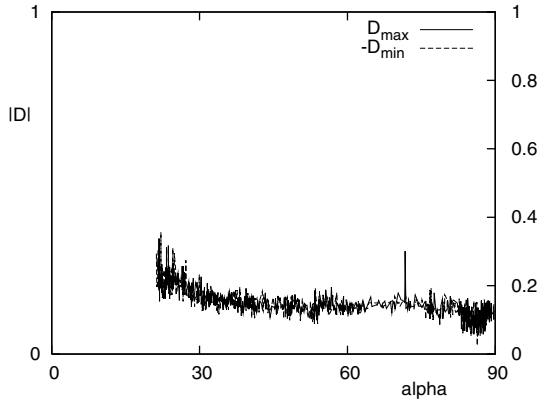

Figure 3. The same as in Fig. 2, except that the Kp4 mask has been applied. This shows that there is far less foreground contamination outside the Kp4 mask. Circles with $\alpha < 21^\circ$ are not displayed, because a too large fraction of each of them is inside the Kp4 mask.

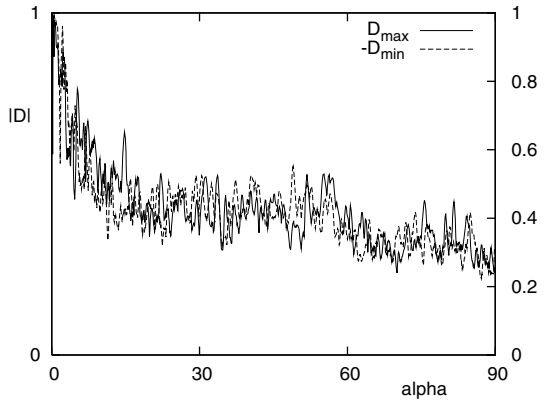

Figure 4. *D* statistic of the ILC map.

the circles, apart from statistical fluctuations. This is in agreement with equation (4), since larger circles sample more independent pixels. On the other hand, front-to-front circles that cross the Galactic plane perpendicular reveal strong correlations resulting from foreground contamination, see Fig. 2. Both, the symmetry between $D_{\rm min}$ and $D_{\rm max}$, and the monotonically decreasing sum $-D_{\rm min} + D_{\rm max}$ are heavily distorted by peaks in $D_{\rm max}$ that result from residual foregrounds. Fig. 3 looks completely different to the former. The only difference in producing it was to apply a galaxy cut. While in Fig. 2 all pixel weights were set equal to 1, in Fig. 3 those inside the Kp4 mask of Bennett et al. (2003) were set to zero which is tantamount to taking only those parts of the circles that are outside the galaxy cut. The symmetry between $D_{\rm min}$ and $D_{\rm max}$, and the monotonically decreasing width of the distribution in Fig. 3 show that there is far less contamination outside the Kp4 mask. Figs 2–8 were all made with the same front-to-front circles, i.e. circles that cross the Galactic plane perpendicular. It is therefore possible to compare these figures directly with each other.

Of interest to the current paper are also the other foreground-reduced maps, i.e. the internal linear combination (ILC), the LILC, and the two TOH maps. We question how reliable these maps are, in particular near to the Galactic plane. With reliable we mean whether there are any correlations from foreground contamination or any systematics from the process of creating the maps. We emphasize that *not all* foreground systematics necessarily result in correlations.

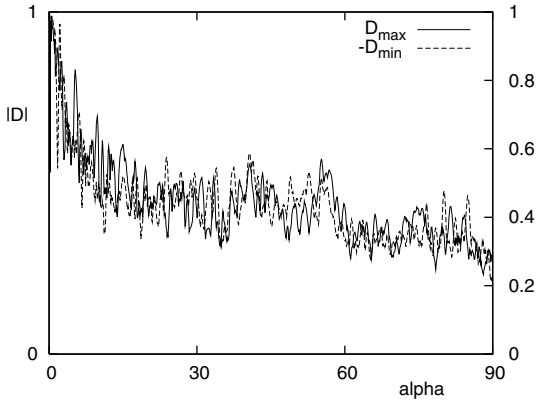

Figure 5. *D* statistic of the LILC map.

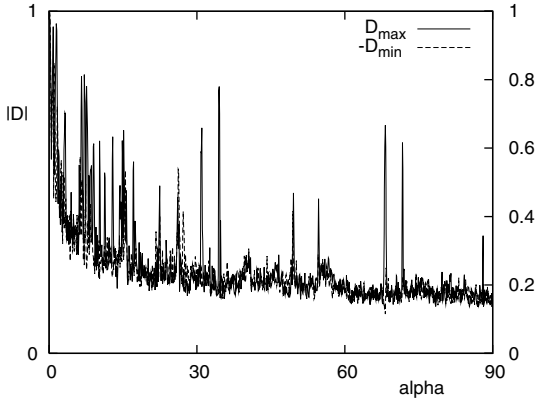

Figure 6. *D* statistic of the TOH map.

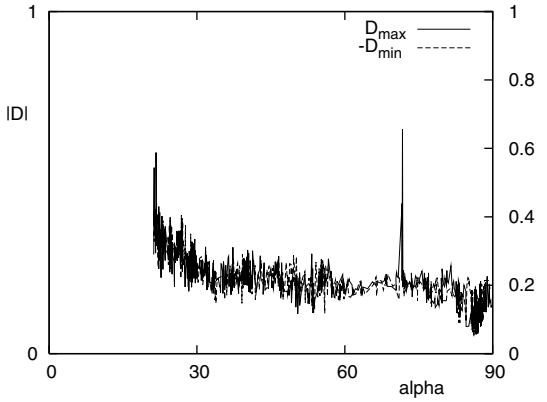

Figure 7. *D* statistic of the TOH map outside the Kp4 mask.

For example, uncorrelated Gaussian noise that contaminates the data will never be recovered with the *D* statistic. However, turning the tables, as soon as we find any correlation, we doubt that the temperature fluctuations are free of residual foreground systematics. Applying masks allows us to locate the foreground-contaminated regions. The only exception is correlations according to the circle-in-the-sky signature. If present, one can circumvent the latter in choosing paths that are not circles.

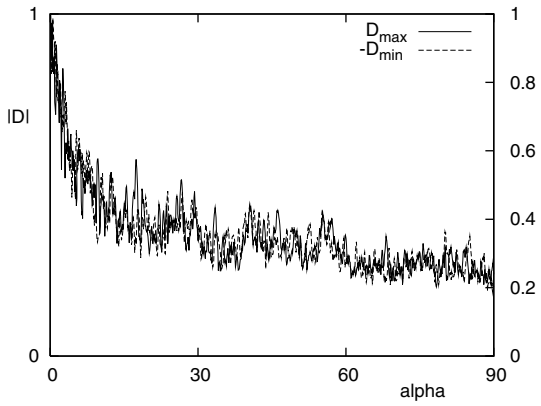

Figure 8. *D* statistic of the Wiener filtered TOH map.

4 CMB MAPS

The following foreground-reduced first year CMB maps are available from the Legacy Archive for Microwave Background Data Analysis (LAMBDA) archive.

(i) The foreground-cleaned *Q*-, *V*- and *W*-bands of the first year *WMAP* data (Bennett et al. 2003) that result from removing the free–free, synchrotron and dust emissions via externally derived CMB template fits. The advantages of these maps are the high resolution, in particular 0.23° for the *W*-band, the well-specified noise properties, and the frequency specific information that is contained in the three microwave bands, *Q*, *V* and *W*.

(ii) The ILC map that is designed to reduce the foreground contamination via weighted combinations of the five *WMAP* bands (Bennett et al. 2003).

(iii) The LILC map of Eriksen et al. (2004) produced with a variant of the ILC algorithm that employs a Lagrange multiplier.

(iv) The reduced foreground TOH map of Tegmark et al. (2003) that results from a variant of the Tegmark & Efstathiou (1996) technique which makes no assumptions about the CMB power spectrum, the foregrounds, the *WMAP* detector noise or external templates. Since the TOH map is free of assumptions about external templates, it has the advantage that it can be used for cross-correlation with, e.g. galaxy and *X*-ray maps. Furthermore, according to Tegmark & Efstathiou (1996), their technique preserves the information on the noise properties of the CMB map. In principle, Tegmark et al. (2003) should be able to specify the noise properties of their map. However, unfortunately, there are no noise properties given for the TOH map.

(v) The Wiener filtered TOH map (Tegmark et al. 2003) which is designed for visualization purposes in order to represent the best guess as to what the CMB sky actually should look like.

Applying the *D* statistic to these maps, we find the following.

(i) The foreground-cleaned *Q*-, *V*- and *W*-band maps are useful for quantitative analyses outside the Kp4 mask, see Fig. 3 and the text in Section 3. Inside the Kp2 mask, these maps should only be used with care, because the templates were fit with data outside the Kp2 mask and the foreground removal is not applicable to regions near to the Galactic plane where the spectrum of the Galactic emission is different. In particular, the maps should never be used inside the Kp4 mask, see Fig. 2.

(ii) According to Bennett et al. (2003), the ILC map is useful for visual presentation of the CMB anisotropy signature and for foreground studies. However, because of the complicated noise correlations, it should not be used for CMB studies. Our finding is that the ILC map is not this bad. Only the distribution of the *D* statistic is very wide, see Fig. 4. The large values of $-D_{\rm min}$ and $D_{\rm max}$ highlight the low resolution of the ILC map, cf. equation (4) and the text in Section 3. Nevertheless, the ILC map has the advantage that it does not require any galaxy cut to be applied. In order to find a symmetry between $D_{\rm min}$ and $D_{\rm max}$ for the ILC map, it is indispensable that the DC component along the front-to-front circles was removed in our analyses. If one would compute the *D* statistic of the ILC map with the DC component included, the symmetry between $D_{\rm min}$ and $D_{\rm max}$ would be distorted. This indicates some bias in the ILC map with respect to the DC component along front-to-front circles.

(iii) The LILC map shows similar results as the ILC map, see Fig. 5.

(iv) The *D* statistic reveals that the TOH contains some residual foreground systematics if one analyses the full sky without any cut, see Fig. 6. These foreground systematics require the Kp4 mask to be applied, see Fig. 7. If compared to the foreground-cleaned *W*-band map of Bennett et al. (2003), see Fig. 3, the distribution of the *D* statistic is slightly wider for the TOH map indicating that the resolution is slightly worse than the claimed 13 arcmin. There is one sharp peak in Fig. 7 at $\alpha = 71.7^\circ$. Less pronounced, this peak occurs also in Fig. 3. The reader, however, is warned not to misinterpret this peak as a detection of a matched circle pair. If the Kp4 mask combined with the point source mask of Bennett et al. (2003) is applied, the sharp peak in Fig. 7 vanishes completely. This tells us that there is some residual foreground contamination outside the Kp4 mask, but inside the point source mask.

(v) The Wiener filtered TOH map shows similar results as the ILC and the LILC map, except that the distribution of the *D* statistic is somewhat smaller which indicates that the resolution of the Wiener filtered TOH map is better than 1°.

5 TOPOLOGY AND CIRCLES IN THE SKY

In the following, we choose a linear superposition of the foreground-cleaned *Q*-, *V*- and *W*-bands of Bennett et al. (2003) as described in Cornish et al. (2004) and use the matched circle test in order to search for signatures of a non-trivial topology. Such searches have already been done for back-to-back circles (de Oliveira-Costa et al. 2004; Roukema et al. 2004; Aurich, Lustig & Steiner 2005c) and have been extended to nearly back-to-back circles (Cornish et al. 2004). In order not to swamp the Sachs–Wolfe effect (SW) by the integrated Sachs–Wolfe effect (ISW), we use the angular weights that have been introduced in Cornish et al. (2004).

Since Cornish et al. (2004), cf. also Shapiro Key et al (2006), have not found any matched circle pair, one could conclude that the Universe has a trivial topology. At this point, it is worthwhile to remember that Roukema et al. (2004) have reported a slight signal for six circle pairs with a radius of $11^\circ \pm 1^\circ$ in the ILC map which they interpret as a possible hint for the left-handed dodecahedral space. While the systematic research for matched circles in spherical spaces carried out by Aurich et al. (2005c) has not found these circles, Aurich et al. (2005c), however, report a marginal hint for the right-handed dodecahedron and for the right-handed binary tetrahedral space, respectively. In addition, there is strong evidence for a finite Universe with a small dimension, because of the anomalies of the large-scale temperature fluctuations which rule out the concordance model with a probability of 99.996 per cent, but could be explained by a multiply connected universe (de Oliveira-Costa et al. 2004). These anomalies are the surprisingly low quadrupole, the quadrupole–octupole alignment, and the planar octupole.

We are not aiming to repeat a back-to-back search. We avoid also to run the full search that has been started by Cornish et al. (2004), because this would require more computer resources than we could ever afford. Instead, we explore whether there are any matched front-to-front circles in the sky that result from orientation preserving isometries. This search has never been carried out before, and it can be done within a few days on a multiprocessor workstation. In our search, we exclude contaminated regions of the CMB sky via the Kp4 and the point source mask by replacing the temperature fluctuations inside these pixels with those given by the ILC map.

One may wonder whether it makes sense to search for front-to-front circles. Are there any topologies that predict front-to-front circles? The surprising answer is *yes*. An example is the Picard universe (Aurich et al. 2004). Choosing the cosmological parameters as was done in Aurich et al. (2004, 2005a), the Picard universe predicts 40 circle pairs of which 23 are front to front. Further details of the Picard topology can be found in Aurich, Steiner & Then (2003); Then (2006). Not only the Picard, but also many other topologies in spherical, flat and hyperbolic space, respectively, predict front-to-front circles, if one allows that the multiply connected space has elliptic fixed points. As another example, see the hyperbolic tetrahedral space investigated by Aurich (1999) and Aurich & Steiner (2001).

Exploring all front-to-front circles of orientation preserving isometries with a HEALPIX resolution of $N_{\rm side} = 256$, we have not found any matched circle pair that can be significantly distinguished from false positive matches. This leads us to the conclusion that there are no matched front-to-front circles on the CMB sky, but care has to be taken since this conclusion is only significant for circles with large radius, $\alpha \gg 45^\circ$. Otherwise, if $\alpha \leqslant 45$, the width of the D-value distribution, cf. equation (4), reaches nearly the height of the D-values that are expected for matched circles (equation 3).

In order to be more specific, we make quantitative estimates for the width of the D-value distribution and for the height of the expected D-values in case of matched circle pairs. The height of the expected D-values for matched circles depends sensitively on the correlation ratio χ of equation (5). The correlated signal in the CMB due to topology comes from the naive Sachs–Wolfe effect. For a circle radius of $\alpha = 45^\circ$, the Doppler effect contributes to the uncorrelated part of the signal. Any other physical effects, e.g. the late integrated Sachs–Wolfe, and the Sunyaev–Zeldovich effect, contribute to the uncorrelated part of the signal, independently of the circle radius. In addition, there are residual foreground contamination and detector noise which are not correlated with respect to the universal covering of the quotient space. Modelling the Universe shows that the contribution of the late integrated Sachs–Wolfe effect plus the contribution of the Doppler effect is of the same order as the contribution of the naive Sachs–Wolfe effect, see fig. 8 in Aurich, Lustig & Steiner (2005b). This results in $A^2_{\rm uncorr} + A^2_{\rm noise} > A^2_{\rm corr}$. Consequently, the correlation ratio is $\chi < 1$. If there would be a matched pair of circles in the sky, we would get a D-value for this matched circle pair which is $D_{\rm peak} < 0.5$, see equation (3). These single D-values, one for each matched circle pair, are embedded in a large number of D-values that are distributed around $D_{\rm peak} = 0$ with a standard deviation of $\sigma \simeq \sqrt{1/N_0}$, cf. equation (4). The largest number of independent pixels that a front-to-front circle can sample in the *WMAP* data is $N_0 = 180^\circ/0.23^\circ = 782$ yielding $\sigma > 0.036$. Due to the large number of 3×10^{11} D-values, namely one for each circle centre times each radius times each relative phase, many of these D-values reach $D_{\rm max} \gg 5\sigma \simeq 0.18$. Among these D-values, $D_{\rm max} \gg 0.18$, it might be possible to find a matched circle that has $D_{\rm peak} < 0.5$, but the risk that matched circles are overlooked among many false positive detections is high. In particular, taking the detection threshold

$$D_{\rm trigger}(\alpha) \simeq \langle S^2 \rangle^{\frac{1}{2}} \sqrt{2 \ln \left(\frac{N_{\rm search}}{2\sqrt{\pi \ln(N_{\rm search})}} \right)}$$

of Cornish et al. (2004) results in a number of false positive detections for front-to-front circles, whereas there is also the risk that even true matched circles may be missed, cf. Aurich et al. (2005c). Here, the main source of trouble is that for front-to-front circles $D_{\rm max}$ is larger by more than a factor of $\sqrt{2}$ if compared to the case of back-to-back circles.

6 THREE-YEAR MAPS

In 2006 March, the NASA Science team has published updated skymaps from 3 yr of *WMAP* data collection (Hinshaw et al. 2006). Repeating our analysis of Section 4 with the 3-yr maps gives the same results as before. This reflects that the *WMAP* observations are stable over the different years.

Also repeating the search of Section 5 does not recover any front-to-front circle in the 3-yr data.

7 CONCLUSION

Analysing CMB maps with D statistics allowed us to specify whether the available maps are contaminated by residual foregrounds. At the same time, D statistics highlighted the angular resolution of the different CMB maps.

We conclude that, at present, the foreground-cleaned Q-, V- and W-band maps of Hinshaw et al. (2006) are the best available maps of the CMB sky. The foregrounds in these maps have been removed with high quality outside the Kp2 mask. Even inside the Kp2 mask, but outside the Kp4 and the point source mask, the foreground reduction is very good. We recommend to use these maps in any quantitative analysis that allows the Kp4 mask to be applied. If one is cautious, it is safe to use the Kp2 mask combined with the point source mask.

Almost as well is the TOH map of Tegmark et al. (2003). It is reliable outside the Kp4 and the point source mask, but its resolution is slightly worse than the claimed 13 arcmin. Unfortunately, the TOH map is yet only available for the first year of *WMAP* data.

The ILC, the LILC and the Wiener filtered TOH map are the only maps that are reliable inside the Kp4 and the point source mask. Unfortunately, because of their low resolution they do not fully meet the requirements of the matched circle test. Their distribution of the S and D statistic is too wide.[1] Nevertheless, they can be used to replace the data of higher resolution maps inside the Kp4 and the point source mask.

Finally, we have searched for matched front-to-front circles, but have not found any.

ACKNOWLEDGMENTS

I thank Dr R. Aurich, S. Lustig and Prof F. Steiner for discussions and helpful comments. Thanks are also to the anonymous referee for

[1] An exception is the search for a given quotient space where several circle pairs are correlated to each other simultaneously. For example, the Poincaré Dodecahedral space predicts six circle pairs. In the simultaneous search, the number of independent pixels along these six circle pairs is six fold, hence narrowing the width of the distribution of the S and D statistic suitably, cf. Roukema et al. (2004), Aurich et al. (2005c).

pointing out that removing the DC component around each circle removes the spurious large correlations. The use of LAMBDA[2] is acknowledged. Support for LAMBDA is provided by the NASA Office of Space Science. The results in this paper have been derived using the CFITSIO[3], the HEALPIX[4] (Górski, Hivon & Wandelt 1999) and the FFTW[5] (Frigo & Johnson 2005) libraries, the GCC compiler and GNUPLOT.

REFERENCES

Aurich R., 1999, ApJ, 524, 497
Aurich R., Steiner F., 2001, MNRAS, 323, 1016
Aurich R., Steiner F., Then H., 2003, in Bolte J., Steiner F., eds, Lecture Notes in Physics, Proc. International School on Mathematical Aspects of Quantum Chaos II. Springer-Verlag, Berlin, preprint (gr-qc/0404020)
Aurich R., Lustig S., Steiner F., Then H., 2004, Class. Quantum Gravity, 21, 4901
Aurich R., Lustig S., Steiner F., Then H., 2005a, Phys. Rev. Lett., 94, 021301
Aurich R., Lustig S., Steiner F., 2005b, Class. Quantum Gravity, 22, 2061
Aurich R., Lustig S., Steiner F., 2005c, MNRAS, 369, 240
Bahcall N. A., Ostriker J. P., Perlmutter S., Steinhardt P. J., 1999, Sci, 284, 1481
Bennett C. L. et al., 2003, ApJS, 148, 97
Cornish N. J., Spergel D. N., Starkman G. D., 1998, Class. Quantum Gravity, 15, 2657
Cornish N. J., Spergel D. N., Starkman G. D., Komatsu E., 2004, Phys. Rev. Lett., 92, 201302
de Oliveira-Costa A., Tegmark M., Zaldarriaga M., Hamilton A., 2004, Phys. Rev. D, 69, 063516
Eriksen H. K., Banday A. J., Górski K. M., Lilje P. B., 2004, ApJ, 612, 633
Frigo M., Johnson S. G., 2005, Proc. IEEE, 93, 216
Górski K. M., Hivon E., Wandelt B. D., 1999, in Banday A. J., Sheth R. K., Da Costa L., eds, Proc. MPA/ESO Conf., Evolution of Large-Scale Structure. PrintPartners Ipskamp, NL, p. 37
Hinshaw G. et al., 2006, ApJ, submitted (astro-ph/0603451)
Roukema B. F., Lew B., Cechowska M., Marecki A., Bajtlik S., 2004, A&A, 423, 821
Shapiro Key J., Cornish N. J., Spergel D. N., Starkman G. D., 2006, preprint (astro-ph/0604616)
Tegmark M., Efstathiou G., 1996, MNRAS, 281, 1297
Tegmark M., de Oliveira-Costa A., Hamilton A. J. S., 2003, Phys. Rev. D, 68, 123523
Then H., 2006, in Cartier P., Julia B., Moussa P., Vanhove P., eds, Frontiers in Number Theory, Physics, and Geometry. Springer-Verlag, Berlin, p. 183

APPENDIX A: ANGULAR WEIGHTS

Searching for the circle-in-the-sky signature in the *WMAP* observations, Cornish et al. (2004) have included angular weights in their S statistic. Namely around each pixel i, they draw a circle of radius α and linearly interpolate values at $n = 2^{r+1}$ points along the circle. They then Fourier transform each circle: $T_i(\phi) = \sum_m T_{im} \exp(\mathrm{i}m\phi)$ and compare circle pairs:

$$S_{ij}(\alpha, \beta) = \frac{2\sum_{m=-2^r}^{2^r-1} |m| T_{im}(\alpha) T^*_{jm}(\alpha) \mathrm{e}^{-\mathrm{i}m\beta}}{\sum_{m=-2^r}^{2^r-1} |m| \left[|T_{im}(\alpha)|^2 + |T_{jm}(\alpha)|^2 \right]}. \quad \text{(A1)}$$

[2] http://lambda.gsfc.nasa.gov/
[3] http://heasarc.gsfc.nasa.gov/docs/software/fitsio/
[4] http://healpix.jpl.nasa.gov/
[5] http://www.fftw.org/

We call this to be angular weights depending on m. β is the relative phase of the two circles and the i, j label the circle centres. The angular weights are important, because otherwise the integrated Sachs–Wolfe effect swamps the Sachs–Wolfe correlations, cf. (Shapiro Key et al. 2006).

Similarly, angular weights can be introduced for the D statistic. They enter as a multiplicative factor on the temperature fluctuations in frequency space.

Definition 2. Let $f(x)$, $\hat{f}(t)$, $u(x)$ and $\hat{v}(t)$ be discrete functions on the points $x, t \in \{0, 1, \ldots, n-1\}$. Let

$$\hat{f}(t) = \mathcal{F}[f](t) = \sum_{x=0}^{n-1} f(x) \mathrm{e}^{-2\pi \mathrm{i} x t/n}$$

be the Fourier transformation and

$$f(x) = \mathcal{F}^{-1}[\hat{f}](x) = \frac{1}{n} \sum_{t=0}^{n-1} \hat{f}(t) \mathrm{e}^{2\pi \mathrm{i} t x/n}$$

its inverse. We call

$$\hat{f}_u(t) := \frac{\mathcal{F}[fu](t)}{\frac{1}{n}\mathcal{F}[u](0)}$$

the u weighted Fourier transform of f, and

$$f_{u,\hat{v}}(x) := \frac{\mathcal{F}^{-1}[\hat{v}\hat{f}_u](x)}{\mathcal{F}^{-1}[\hat{v}](0)}$$

the u, $\hat{v}$ weighted of the function f.

The u weighted Fourier transform at $t = 0$ results in the arithmetic mean of f with respect to the weights

$$\frac{1}{n}\hat{f}_u(0) = \frac{\sum fu}{\sum u} =: \bar{f}.$$

We call $\bar{f}$ to be the DC component of f, and

$$\frac{1}{n}\hat{f}_u(-1)\mathrm{e}^{-2\pi \mathrm{i} x/n}, \quad \frac{1}{n}\hat{f}_u(1)\mathrm{e}^{2\pi \mathrm{i} x/n}$$

to be the lowest frequency AC components of f with respect to the weights.

We remark that the $u = 1$ weighted Fourier transform of f coincides with the Fourier transform of f, i.e. $\hat{f}_1(t) = \hat{f}(t)$. The same is true if $u(x)$ is some other non-zero constant.

The 1, 1 weighted of f coincides with itself, $f_{1,1}(x) = f(x)$. The same is true if $u(x)$ and $\hat{v}(t)$ are some other non-zero constants.

The u weights enter as a multiplicative factor in coordinate space

$$f_{u,1}(x) = \frac{f(x)u(x)}{\frac{1}{n}\sum u}.$$

The $\hat{v}$ weights enter as a multiplicative factor in frequency space

$$f_{1,\hat{v}}(x) = \frac{\mathcal{F}^{-1}[\hat{v}\hat{f}](x)}{\mathcal{F}^{-1}[\hat{v}](0)} = \frac{(v * f)(x)}{\frac{1}{n}\sum \hat{v}}.$$

If we choose f to be the discretization of the temperature fluctuations δT along the curve γ,

$$f(x) := \delta T(\gamma(\phi))_{|\phi = 2\pi\frac{x}{n}}, \quad x \in \{0, 1, \ldots, n-1\},$$

and u to be given by the corresponding pixel weights, see Definition 1,

$$u(x) := \sqrt{w(\gamma(\phi)) \left| \frac{\mathrm{d}}{\mathrm{d}\phi}\gamma(\phi) \right|_{|\phi = 2\pi\frac{x}{n}}},$$

we can take

$$\hat{v}(t) = \hat{v}(-t), \quad t \in \left\{ 0, 1, \ldots, \frac{n}{2} \right\} \quad \text{(for } n \text{ even)},$$

to be real-valued angular weights.

Replacing $\delta T(\gamma_i)$ $(i = 1, 2)$ by its u, $\hat{v}$ weighted in Definition 1, equation (2), we end up with the D statistic that includes both, pixel and angular weights.

If one chooses the curves γ_1 and γ_2 to be circles of the same radius α, sets all pixel weights equal to $w = 1$, and sets the angular weights equal to $\hat{v}(m) = \sqrt{(m)}$ for $m = 0, 1, \ldots, 2^r$, one recovers equation (A1) as a special case of the D statistic.

When using angular weights, one has to be aware that they interact with the angular resolution of the map in dependence of the curves γ. For example, smoothing the map with a Gaussian beam of root mean square σ in radians is the same as multiplying the expansion coefficients a_{lm} of the map with

$$\mathrm{e}^{-l(l+1)\frac{\sigma^2}{2}}.$$

A similar result happens, if one chooses γ_1 and γ_2 to be circles of radius α and applies the angular weights

$$\hat{v}(l) = \mathrm{e}^{-l(l+1)\frac{\sigma^2}{2\sin^2\alpha}}.$$

The difference is that the latter smoothes the map only in the direction along the circles.

Entering in coordinate and frequency space, respectively, the pixel and angular weights interfere. Consequently, we avoid using pixel and angular weights simultaneously. If not otherwise stated, we use pixel weights. The only exception is that we always remove the DC and the lowest frequency AC components of the temperature fluctuations, i.e. we replace δT by

$$\delta T(\gamma(\phi)) - \frac{1}{n}\sum_{t=-1}^{1} \widehat{\delta T}_u(t)\mathrm{e}^{\mathrm{i}t\phi}$$

in Definition 1, equation (2).

This paper has been typeset from a TEX/LATEX file prepared by the author.